Cold Regions Science and Technology 186 (2021) 103277

Contents lists available at ScienceDirect

Cold Regions Science and Technology

journal homepage: www.elsevier.com/locate/coldregions

Water and salt migration mechanisms of saturated chloride clay during freeze-thaw in an open system

Jianpeng Liu [a,b], Ping Yang [a,*], Zhaohui (Joey) Yang [b]

[a] College of Civil Engineering, Nanjing Forestry University, Nanjing, Jiangsu Province 210037, China
[b] Dept. of Civil Engineering, University of Alaska, Anchorage, AK 99508, USA

ARTICLE INFO

Keywords:
Saline soils
Freeze-thaw
Water-salt migration
Matric suction
Water molecule mobility

ABSTRACT

Water and salt migration mechanisms are of great significance for understanding the frost heave and thaw settlement of saline soils during freeze-thaw (F-T). In this study, unidirectional open-system F-T tests were conducted on saturated clay specimens with various chloride salt contents to investigate water and salt migration mechanisms. Relevant parameters, including temperature, unfrozen water content, bulk electrical conductivity, matric suction, and water intake volume, were measured continuously during testing. Besides, the water molecule mobility was obtained by the Nuclear Magnetic Resonance relaxometry tests to help understand the water and salt migration mechanisms. The test results indicated that the freezing front development was highly dependent on salt content. The matric suction gradient was found to be the driving force of water-salt migration, which was larger in specimens with lower salt content and led to more water intake. The migration of water and salt was asynchronous due to their different driving mechanisms during F-T. Specifically, salt migration was affected by both convection and diffusion, while water migration was primarily driven by convection. This phenomenon was also confirmed by the different patterns in water and salt redistributions after F-T. Meanwhile, pore water in the frozen specimens with different salinity and the same unfrozen water content was found to have the same water molecule mobility. Both the matric suction and water molecule mobility were dependent on unfrozen water content but independent on salt content. However, the salt content has a significant effect on the soil freezing point depression, which further affects the matric suction and water molecule mobility.

1. Introduction

Artificial ground freezing (AGF) is a construction technique that circulates chilled coolant in buried pipes to freeze soils, providing water proof and enhancing soil strength before underground excavations. AGF is widely used in underground engineering (Braun et al., 1979; Jessberger, 1980; Fan and Yang, 2019) and has potential in contaminant isolation (Wagner, 2013; Tang et al., 2019). However, the application of AGF usually brings engineering problems such as frost heave (John, 1981; Cai et al., 2019) and thaw settlement (Morgenstern and Nixon, 1971; Chamberlain, 1981; Wang et al., 2019). Moreover, the soluble salts, such as NaCl, widely existing in the coastal area, lower soil freezing point (Banin and Anderson, 1974; Bing and Ma, 2011; Wan and Yang, 2020), which requires low-temperature brine to form a frozen wall with an adequate thickness (Wallis, 1999).

The water and salt migration alters soil pore structure and its compressibility, which are the primary causes of deformation after F-T (Fan et al., 2019). Water migrates to the freezing front under the effect of matric potential gradient during freezing (Wen et al., 2011; Lu et al., 2018), while salt migrates with water driven by two mechanisms: a convective flow of salt toward the freezing front and diffusion in the opposite direction owing to concentration gradients (Stähli and Stadler, 1997). F-T tests in a close system revealed that the amount of water migration from the unfrozen zone to the freezing front depends on the initial solute concentration (Watanabe et al., 2001). Rui et al. (2019a) reported that the migration of water and salt increased with increasing salt concentration; the farther from the freezing front, the smaller amount of water and salt migration during freezing. Taber (1930) first considered the effect of water supplement on F-T tests, and further studies by open-system F-T tests identified some phenomena different from the closed-system F-T tests. The water and salt redistribution after F-T cycles shows that the moisture content increased in the frozen zone but decreased in the unfrozen zone, due to the temperature gradient and matric potential gradient (Bing and He, 2008; Bing et al., 2015).

* Corresponding author at: No. 159 Longpan Road, College of Civil Engineering, Nanjing Forestry University, Nanjing, Jiangsu Province 210037, China.
E-mail addresses: ljp@njfu.edu.cn (J. Liu), yangping@njfu.edu.cn (P. Yang), zyang2@alaska.edu (Z.(J. Yang).

https://doi.org/10.1016/j.coldregions.2021.103277
Received 11 September 2020; Received in revised form 3 March 2021; Accepted 7 March 2021
Available online 16 March 2021

Meanwhile, the ions content in the unfrozen zone rose with a decreasing distance to the freezing front and remained almost unchanged in the frozen zone. It is common to assume that, in the frozen zone, the water flux is zero, and the unfrozen water content drops with decreasing temperature (Loch and Miller, 1975). However, the water and salt migration in frozen saline soils cannot be ignored since the soluble salt can significantly lower the pore water freezing point and result in a significant amount of unfrozen water content even at subfreezing temperatures (Xu et al., 1995). Xiao et al. (2017) found an increase in salt content in the frozen zone due to salt migration during freezing. Wang et al. (2016) proposed a mass balance method to estimate the mean values of water and solute fluxes in soils during freezing. Besides, Wan et al. (2019) conducted laboratory tests to simulate salt transfer under freezing conditions and examine the role of salt transport in sodium sulfate soil.

Researchers proposed that the temperature gradient and water potential gradient (defined as the sum of gravitational potential, matric potential, and osmotic potential) were the main driving forces of water and salt migration (Campbell, 1988; Sarsembayeva and Collins, 2017; Zhang et al., 2019). Drotz et al. (2009) further quantified the contributions of matric and osmotic potentials to the unfrozen water content of frozen saline soils by theoretical models. Various sensing techniques have been utilized to collect data for analyzing the water and salt migration driving mechanisms. Lu et al. (2018) used pF meters to measure the matric suction of frozen soils during F-T and explored its relationship with unfrozen water content and deformation. The salt content was found to have an insignificant impact on the matric suction (Zhang et al., 2017c). Additionally, Wang et al. (2018b) used Computed Tomography images acquired during freezing experiments to demonstrate that the inner cracks and gaps between irregular polygons provided pathways for water migrating from the unfrozen zone to the frozen zone. The influence of initial concentration on the salt redistribution was found to depend on the medium particle size (Huang et al., 2019). Notably, electromagnetic sensors make it possible to continuously monitor the water and salt migration and better characterize the F-T process (Lundin and Johnsson, 1994; Zhang et al., 2017a; Lu et al., 2018; Rui et al., 2019b; Kelleners, 2020). Volumetric unfrozen water content and bulk electrical conductivity were typically measured to analyze the variation of water and salt (Xiao and Lai, 2018).

In summary, limited investigations exist on the water and salt migration mechanisms of saline soils during both freezing and thawing. The objective of this study is to gain an in-depth understanding of the water and salt migration mechanism of saline soils by continuous monitoring during F-T. A series of unidirectional open-system F-T tests were performed on soil specimens with various chloride salt contents. The temperature distribution, unfrozen water content, bulk electrical conductivity, matric suction, and water intake volume were simultaneously measured during the tests. The test results were analyzed to shed light on salt contents' influence on the water and salt migration of saline soils. Meanwhile, Nuclear Magnetic Resonance (NMR) relaxometry tests were conducted to obtain the characteristics of mineral-water interaction to further demonstrate the water and salt migration mechanism.

2. Materials and methods

2.1. Specimen preparation

The soil was sampled from a coastal city in east China, where clayey soils are widely distributed. Fig. 1 shows its grain-size distribution obtained by a laser particle analyzer (Microtrac S3500, USA). According to the Standard for Soil Test Method of China (GB/T 50123-2019, 2019), the soil specific surface area (m^2/g), specific gravity (dimensionless), liquid limit (%), plastic limit (%), and plasticity index were determined to be 22.4, 2.7, 34.7, 21.2, and 13.5, respectively. Based on these index properties, the soil was classified as lean clay (CL) according to the unified soil classification system. The dominant ions in the soil are Na^+/K^+, Ca^{2+}, Mg^{2+}, Cl^-, and SO_4^{2-} with contents (ion mass/dry soil mass) of 0.056%, 0.040%, 0.013%, 0.040%, and 0.096%, respectively. The influence of the Na^+ and Cl^- contents on the freezing point of the original soil was ignored due to their low concentrations.

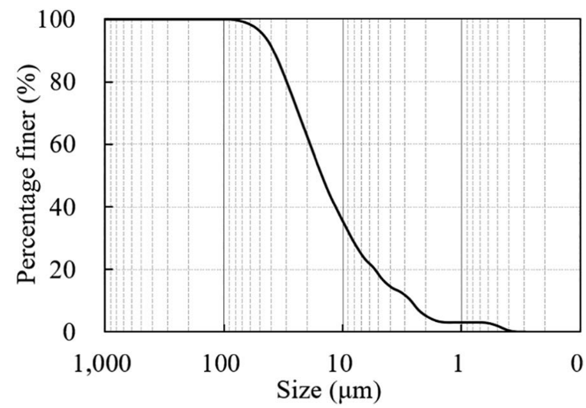

Fig. 1. Soil grain-size distribution for the tested soil samples.

The oven-dried soil was pulverized to yield particles smaller than 2 mm in diameter. Subsequently, the dry soils were compacted into the mold with a diameter of 20 cm in six layers of 5.5 cm thick per layer to achieve a certain dry density of 1.5 g/cm^3. Then, the soil samples were vacuum saturated and consolidated under 200 kPa simulating the effective overburden pressure at about 20 m below the ground surface. Note that the saturation media was NaCl solution with a concentration of 0 mol/L, 0.64 mol/L, 1.32 mol/L, or 2.64 mol/L, corresponding to the salt content (s = salt mass/dry soil mass) of 0%, 1%, 2%, or 4%, respectively. The final specimens had a diameter of 20 cm, a height of 30 cm (± 0.3 cm) with a dry density of 1.65 g/cm^3, and the degree of saturation was determined to be higher than 95%. It is noteworthy that the dry density of the prepared specimens, i.e., 1.65 g/cm^3, is consistent with that of the in-situ undisturbed soils. The volumetric water content of the prepared soil specimens was 0.416 m^3/m^3, corresponding to a gravimetric water content of 25.2%. The initial freezing points (T_f) of soil specimens were obtained through freezing point tests as shown in Fig. 2 and identified to be −0.7 °C, −2.8 °C, −5.0 °C, or − 11.0 °C for the specimen with a salt content of 0%, 1%, 2%, or 4%, respectively. In addition, the preparation method of specimens for the NMR relaxometry tests and their physical properties (such as density, moisture content, salt content, and degree of saturation) were the same as those for the F-T test described above, except that the NMR relaxometry test specimens had a diameter of 2.4 cm and a height of 5.5 cm. More details of the specific preparation procedure can be found in Liu et al. (2020a).

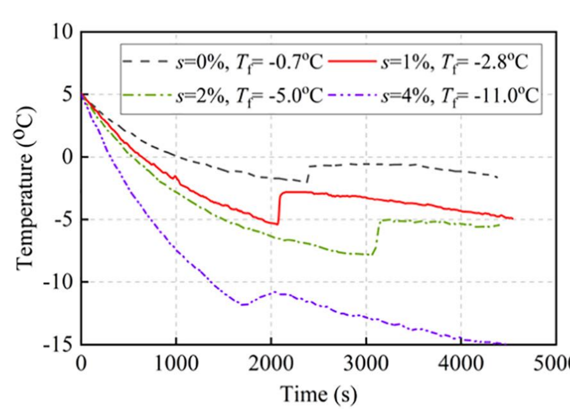

Fig. 2. The cooling curves of saline soils.

2.2. Test apparatus

Fig. 3 illustrates the custom-designed F-T test apparatus. To simulate the freezing conditions in AGF engineering, the cold end was placed at the bottom of the apparatus (Fan et al., 2019). In particular, seven thermometers, two 5TE sensors, and two matric suction sensors (TEROS 21, also known as MPS-6) were installed along the sample height of this apparatus to monitor the temperature, unfrozen water content, bulk electrical conductivity, and matric suction during F-T. A total of seven thermometers, evenly spaced within a height of 4.5 cm, were installed to obtain temperature distribution along the specimen. Among them, two thermometers, e.g., Th-2 and Th-5, coincided with the axes of the bottom and top matric suction sensors, respectively. Two 5TE sensors (refer to the insert in Fig. 3) with three-pronged probes (10.0-cm long × 3.2-cm wide × 0.7-cm thick) were installed along the radial direction 10 cm apart to measure the unfrozen water content and bulk electrical conductivity. In principle, the 5TE sensor applies an electromagnetic field in the surrounding soil and measures its apparent dielectric permittivity, which is then used to estimate the unfrozen water content (Decagon Devices, 2010). In addition, the bulk electrical conductivity is obtained by applying an alternating electrical current to two of the three electrodes and measuring the resistance between them. The matric suction sensor (9.6-cm long × 3.5-cm wide × 1.5-cm thick) has a measuring range of −9 kPa to −100,000 kPa and an accuracy: ±10% of reading from −100 to −9 kPa (Walthert and Schleppi, 2018). Note that the sensor was not sufficiently calibrated beyond −100 kPa, and the absolute value of the measured results was used for analyses in this study. Matric suction sensors and 5TE sensors were installed on opposite sides to reduce the sensor size effects on water and salt migration. All sensors were installed after the sample preparation by digging holes along the specimen. Any gaps left were backfilled with the excavated soil after inserting sensors. And the wet soil was firmly packed around the sensing part of the matric suction sensor, i.e., the ceramic disc (Fig. 3), before installation to ensure good surface contact. The water supply device was a coiled tube with a diameter of 4 mm, as shown in Fig. 3, which provided a higher measurement accuracy than a Mariotte bottle (Zhou et al., 2014).

The characteristics of water molecule mobility were monitored by a NMR relaxometry apparatus, a MesoMR23-060 V-I system produced by Niumag Corporation, China. The apparatus consists of a testing chamber, a temperature-controlling system with a test temperature range between -25 °C and 25 °C and accuracy of 0.05 °C, a radio frequency system, and a data acquisition and analysis system.

2.3. Experimental program

Soil specimens were pre-cooled in an environmental chamber at 2 °C for 12 h after sensor installation, allowing the ceramic disc to achieve hydraulic equilibrium with the surrounding soil. Subsequently, the freezing process started with the cold end set to -15 °C, the warm end set to 2 °C, and the environmental chamber maintained at 2 °C. The soil specimens with different initial salt contents were subjected to a freeze-thaw cycle with a supply of NaCl solutions of the same salt concentrations as the specimens. A relatively low freezing temperature (i.e., −15 °C) was adopted to account for the depressed freezing points of saline soils, which is consistent with engineering practices (Wallis, 1999). The freezing process lasted for 60 h to achieve thermal equilibrium, which corresponded to a stabilized temperature at each monitoring point. The water intake volume measurement was terminated at the end of the freezing process. The specimen was allowed to thaw by setting the environmental chamber to 25 °C and disconnecting the cryostats for 12 h typically. A pressure of 7 kPa was applied for counteracting the friction between the specimen and its container during thawing. The temperature, volumetric unfrozen water content, bulk electrical conductivity, and matric suction data were recorded automatically once every 3 min during F-T, and the volume of water intake was recorded manually once every 30 min during freezing. After a F-T cycle, the gravimetric water content and salt content were re-examined by sampling the specimens in seven layers evenly distributed along the specimen height. The gravimetric water content was determined by the oven-drying method, and the NaCl content was determined by examining the solution obtained from 8 g air-dried soil diluted in 40 mL deionized water (GB/T 50123-2019, 2019).

The NMR relaxometry test aimed to obtain the water molecule mobility during F-T, which can help reveal the water and salt migration mechanism. The test was conducted in soils with the same salt contents as those in the F-T tests, and the specimens were step-cooled in the NMR chamber for at least 4 h to ensure a uniform temperature distribution. In

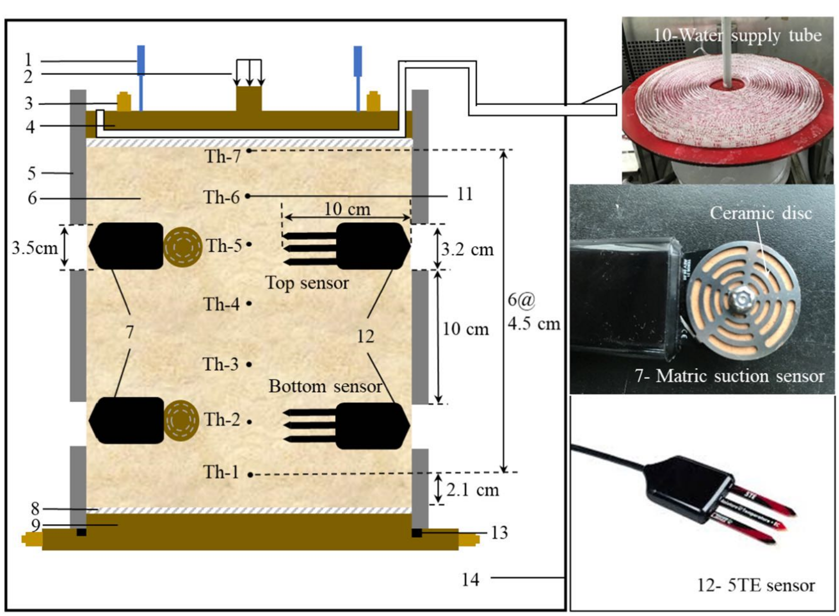

Fig. 3. Schematic of the F-T testing system and sensor installation, showing 1 - displacement transducer; 2 - loading system; 3 - inlet/outlet coolant; 4 - warm plate; 5 - specimen tube; 6 - soil specimen; 7- matric suction sensor; 8 - bronze porous disc; 9 - cold plate; 10 - water supply device; 11 - thermometer along the vertical axis of the specimen; 12 - 5TE sensor; 13- sealing rubber ring; and 14 - environmental chamber.

the NMR measurements, the longitudinal proton relaxation time (T_1) and the transverse proton relaxation time (T_2) result from the interaction between protons in the fluid and between the protons in the fluid and the pore surface, respectively. The T_1-T_2 correlation spectra obtained with the IR (Inversion Recovery)-CPMG (Carr-Purcell-Meiboom-Gill) sequences is an effective way to characterize the pore water molecule mobility (Tian et al., 2019a).

3. Results and analyses

3.1. Heat transfer

Temperature variation at various locations within the specimen is a great and direct indicator of the F-T process. At the same temperature boundary conditions (i.e., −15 °C at the cold end and 2 °C at the warm end, or a temperature gradient of 0.57 °C/cm along the specimen height), the temperature sequences for specimens with different salt contents share the same pattern. For instance, Fig. 4 illustrates the temperature change at various heights of the specimen with 4% salt content during F-T. The three stages, i.e., pre-cooling, freezing, and thawing, are labeled in the figure. One can see that the temperature stabilized at the 33rd hour until thawing started at the 72nd hour. And thawing occurred much faster than unidirectional freezing due to heat transfer in all directions.

The location of the freezing front is important as it serves as the boundary separating the frozen zone from the unfrozen zone. At the thermal equilibrium state, the freezing front was located according to the freezing point of an individual specimen (refer to Fig. 2) by linear interpolation of the measured temperature distribution. Previous studies showed that the temperature distribution during unidirectional freezing was linear in the section close to the cold end and curve-linear near the warm end at the unsteady state (Zhang et al., 2017b; Zhang et al., 2018). Therefore, the location of the freezing front at the unsteady state was also determined by linear interpolation due to its proximity to the cold end in the early stage of freezing. Fig. 5 illustrates the evolution of the freezing front location, i.e., distance from the cold end (H_F), with time. H_F is also the same as the frozen zone height in this case. One can see that the freezing front moved faster at the beginning of freezing and then gradually reached a plateau (i.e., thermal equilibrium) at the end of the freezing process. In the fast-moving stage, the freezing front of specimens with a higher salt content moved slower than that with lower salt content, due to the freezing point depression induced by salt. In the steady stage, the final location of the freezing front depended on salt content, and the soil specimen with a lower salt content had a freezing front farther away from the cold end. Moreover, salt migrated with water toward the cold end, and was repelled from ice during pore water freezing. Therefore, the salt concentration increases near the freezing front, which further restrained its upward movement.

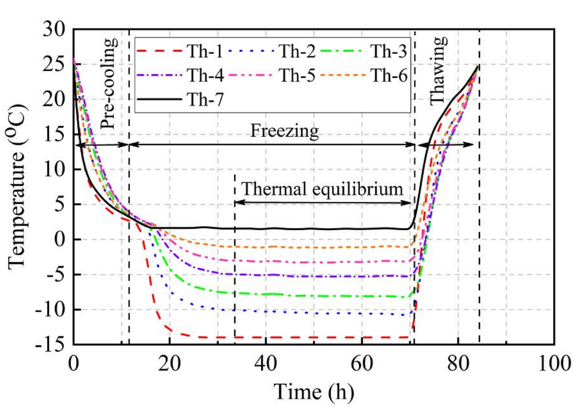

Fig. 4. Temperature vs. time during freeze-thaw of soil specimen with 4% salt content.

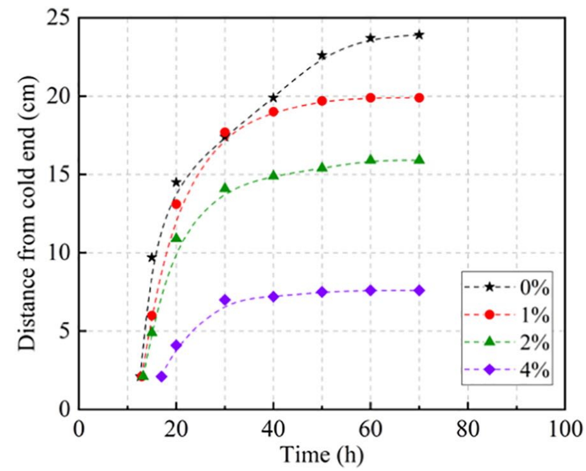

Fig. 5. Evolution of the freezing front with time for specimens with different salt contents.

3.2. Water and salt migration

The pore water molecule mobility measured by the NMR relaxometry was used to characterize the mineral-water interaction, which played an important role in water and salt migration. The volumetric unfrozen water content (θ_u), bulk electrical conductivity (σ_b), and matric suction (ψ_m) were obtained in the unidirectional open-system F-T tests. The θ_u was calculated based on the measured apparent dielectric permittivity according to the equation proposed in Liu et al. (2020b) and used to investigate water migration. Meanwhile, the σ_b was directly utilized to characterize salt migration. In addition, the ψ_m was measured to help analyze the driving force of water and salt migration.

3.2.1. Water molecule mobility

As shown in Fig. 6, results obtained from specimens of two salt contents at four temperatures were selected to illustrate the representative stages of the T_1-T_2 correlation spectra during F-T and the impact of temperature and salt content. Specifically, four temperatures were picked, as indicated in Fig. 6, including a temperature above T_f, two lower than T_f with decreasing unfrozen water content during freezing, and one during thawing. Notably, one temperature below freezing point from each specimen (e.g., −3.5 °C of 1% salt content and −7.2 °C of 2% salt content) was chosen so that similar unfrozen water contents were present to analyze the effect of temperature and salt content on the water molecule mobility. The T_1/T_2 ratio is a characteristic parameter accounting for molecule mobility (Tian et al., 2019a; Tian et al., 2019b), which can be used to explain the water-salt migration mechanism. The Bloembergen-Purcell-Pound (BPP) model suggests that the free water molecule undergoing isotropic molecular tumbling without interacting with a solid surface exhibits a T_1/T_2 ratio of 1.0, whereas the T_1/T_2 ratio exceeding 1.0 indicates decreased water mobility due to the water-solid interaction (Bloembergen et al., 1948). Notably, the T_1-T_2 correlation spectra in Fig. 6 show a single peak (yellow spectrum indicated the peak value), while the spectra in Ohkubo et al. (2016) and Tian et al. (2019a) had two peaks. The differences are possibly due to soil specimen preparation methods. Two peaks in the spectra in the cited references demonstrated two distinct environments for the pore water, which was likely caused by the layer-by-layer compaction method adopted for specimen preparation. Only one peak was revealed in this study, indicating a consistent pore water environment afforded by the uniform pore structure resulted from specimens prepared by the consolidation method.

The T_1/T_2 ratio generally increased with decreasing temperature below T_f during freezing and decreased with increasing temperature until it was completely thawed during thawing. It indicated that T_1/T_2

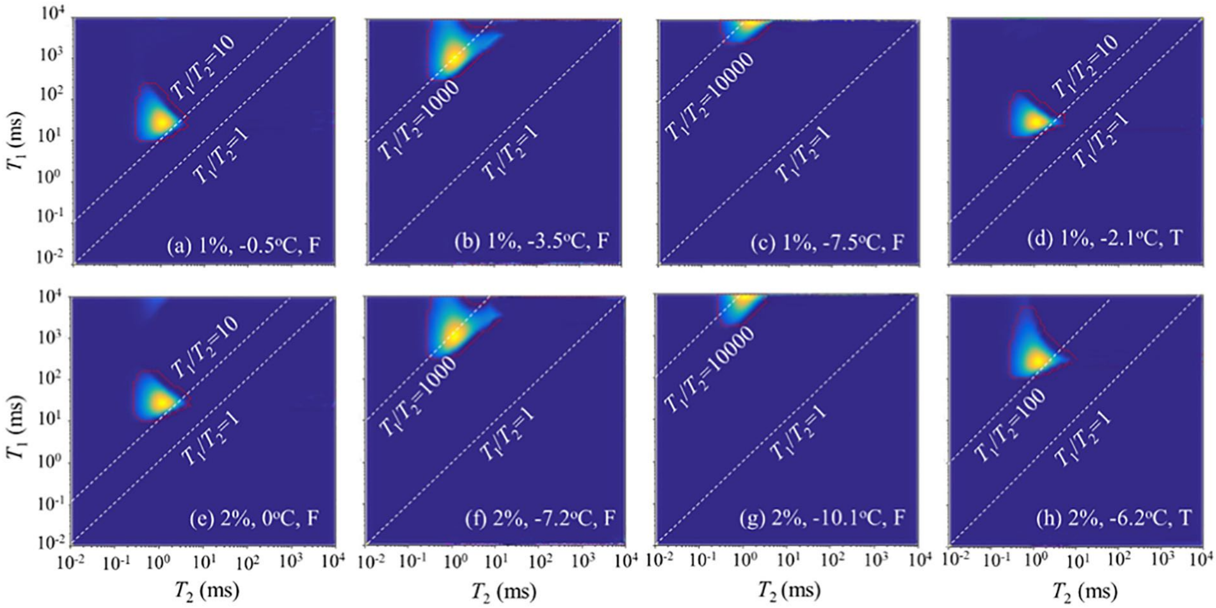

Fig. 6. T_1-T_2 correlation spectra for specimens with different salt contents: (a) through (c) for 1% salt content and (e) through (g) for 2% at varying temperatures during freezing; (d) for 1% and (h) for 2% during thawing.

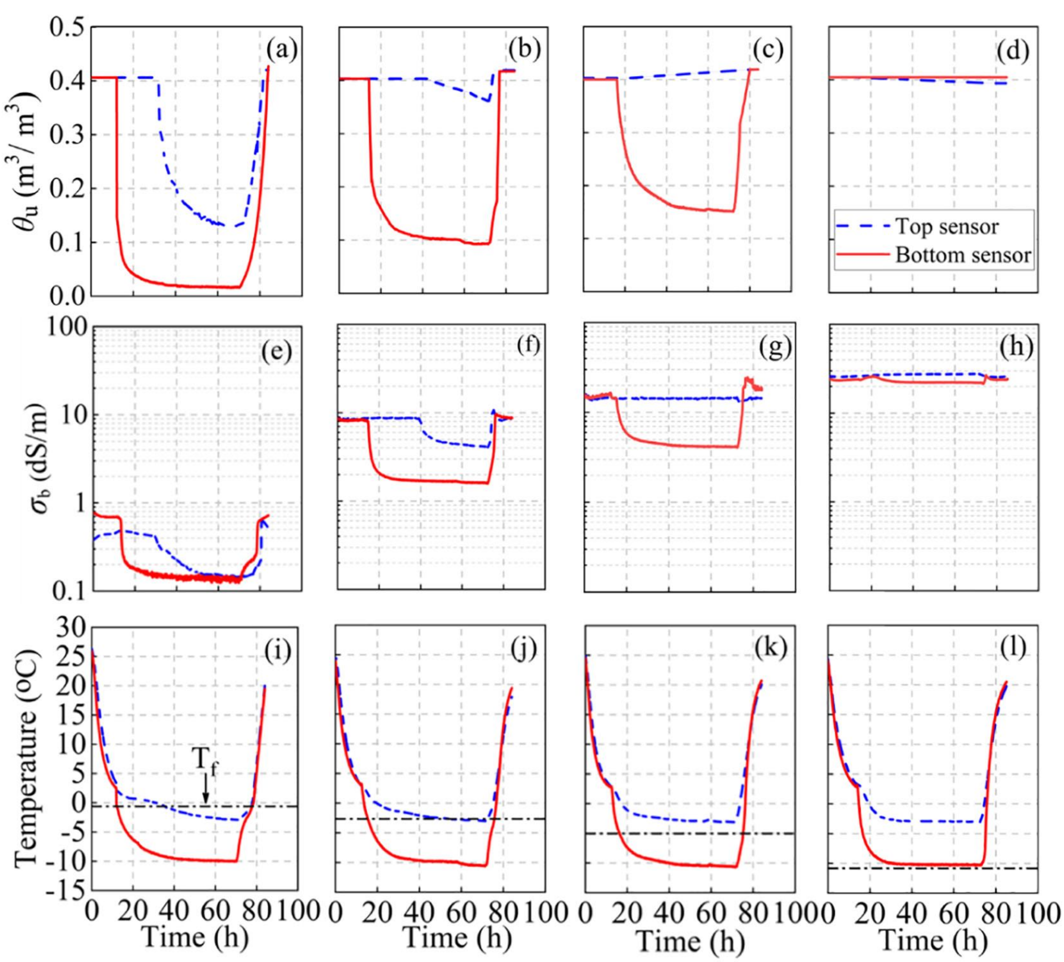

Fig. 7. Unfrozen water content, bulk electrical conductivity, and temperature vs. time during F-T for specimens with various salt contents: (a), (e), and (i): no salt; (b), (f), and (j): 1% salt content; (c), (g), and (k): 2% salt content; and (d), (h), and (l): 4% salt content. Note that the horizontal dashed lines in the temperature vs. time plots indicate the soil specimen's initial freezing points.

ratio was dependent on θ_u, instead of temperature. The larger T_1/T_2 ratio at temperatures lower than T_f demonstrated significantly lower water molecule mobility at lower θ_u, which caused less water-salt migration. From Fig. 6a and e, one can see that the peak T_1/T_2 ratios of soil specimens with different salt contents were about the same and close to 10. This result indicated the T_1/T_2 ratio was independent of salt content at an unfrozen state. In the frozen state, by comparing Fig. 6b with f, the peak T_1/T_2 ratios for both specimens were found to be around 1000. As presented in Liu et al. (2020b), the θ_u was 0.326 m^3/m^3 at -3.5 °C in 1% salt content and 0.331 m^3/m^3 at -7.2 °C in 2% salt content. It revealed that pore water in soil specimens with the same θ_u had the same pore water molecule mobility regardless of salt content, consistent with the findings in Ohkubo et al. (2016) and Tian et al. (2019b). In other words, the existing soluble salt was not directly related to the water molecule mobility. Rather, it lowered the freezing point, hence influencing the unfrozen water content and then the water molecule mobility during F-T.

3.2.2. Unfrozen water content and bulk electrical conductivity

Continuous monitoring of θ_u and σ_b helps reveal water and salt migration during F-T. Fig. 7 shows the variation of measured θ_u, σ_b, and temperature for specimens with different salt contents at two sensor locations (i.e., bottom and top) in the unidirectional open-system F-T tests. Notably, for thermal couples shown in Fig. 3, the bottom sensor refers to Th-2, and the top sensor refers to Th-5. As indicated by the temperature data in relation to the freezing point of each specimen, the freezing front reached and passed both the bottom and top 5TE sensors in specimens with 0% and 1% salt content, while it only passed or approached the bottom sensors in specimens with 2% or 4% salt content. From the soil specimen with no salt in Fig. 7a and i, one can see that θ_u decreased rapidly once the freezing front arrived at the bottom sensor and then gradually dropped and became almost constant, as the freezing front moved upward until the specimen started to thaw. This trend can also be noticed in the θ_u at the top sensor, except that the gradual decrease lasted through the rest of the freezing. Since more θ_u existed at relatively high subfreezing temperatures, leaving more channels for water and salt migration. This phenomenon can also be identified in saline soil specimens. For the specimens with various salt contents (Figs. 7b, c, and d), the measured θ_u values at both the bottom or top sensors increased with increasing salt content in the thermal equilibrium state. For example, θ_u measured by the bottom sensor increased from 0.017 m^3/m^3 to 0.093 m^3/m^3, 0.152 m^3/m^3, and then 0.405 m^3/m^3 when the salt content of specimens rose from 0% to 1%, 2%, and 4%, respectively.

Monitoring of unfrozen water content during F-T revealed water migration patterns. One can easily observe that θ_u at both the bottom and top sensors increased after F-T for all but the specimen with 4% salt content. The increase in θ_u occurred for the specimen without salt, from 0.406 m^3/m^3 to 0.427 m^3/m^3 or with an increasing amplitude of 5.2% at the bottom sensor. It indicated a significant amount of water migration during F-T. The variation of θ_u measured in the unfrozen zone, including the top sensor for 2% salt content and both sensors for 4% salt content, directly demonstrated the water migration process during F-T. As illustrated in Fig. 7c, one can see from the θ_u measured by the top sensor that the water content increased by 0.016 m^3/m^3 after a F-T cycle. It is shown that water from the warmer end and supplied water migrated toward the freezing front, and the outgoing water flux was less than the incoming water flux. However, the θ_u for the specimen with 4% salt content was almost unchanged at the bottom sensor, and that at the top sensor decreased by 0.009 m^3/m^3. This result figured out that the outgoing water flux was the same as the incoming at the bottom sensor at the location close to the freezing front. In contrast, unbalanced water fluxes were identified at the top due to the fact that it was far from the freezing front, and the convection was dominant. In the following section, the driving force of the convection will be further discussed.

The variation of σ_b of soil specimens with different salt contents during F-T shown in Fig. 7f through h helps understand the salt migration. Note that the σ_b of soil specimen with no salt was illustrated to demonstrate to high sensitivity of 5TE sensors (Fig. 7e). This study assumed that no crystallization of NaCl occurred since the temperature was above -15 °C (Xu et al., 1995). The initial σ_b values measured at the bottom and top sensors were very close, confirming uniform salt distribution within the prepared soil specimens. Moreover, the initial σ_b increased with increasing salt content. Specifically, it increased from around 0.5 dS/m to 8.6 dS/m, 15.2 dS/m, and then 24.5 dS/m when the salt content increased from 0% to 1%, 2%, and 4%, respectively. Comparing the variation of σ_b with θ_u, for the specimen with 1% salt content (Fig. 7b and f), one can see that the σ_b and θ_u at the bottom varied synchronously, whereas σ_b decreased earlier than θ_u at the top. This phenomenon was caused as the pore water at the bottom quickly froze, resulting in the simultaneous change of both unfrozen water content and bulk electric conductivity. However, the pore water viscosity increased when the top portion of the specimen gradually cooled, but the temperature remained above the freezing point. Therefore, a gradual decrease in σ_b was identified while the θ_u stilled remained unchanged.

At subfreezing temperatures, one might expect the measured σ_b to increase since the salt concentration increased due to decreased θ_u. However, the opposite occurred, as the conductivity pathways were blocked by ice crystals (Liu et al., 2020b). The variation of σ_b was different from that of θ_u during thawing, too. For example, σ_b of the specimen with 1% salt content increased quickly and then decreased slightly, as shown in Fig. 7f. This can be explained as follows: at the onset of thawing, more conductivity pathways were created with an increasing θ_u as ice crystals melted to allow the pathway to reconnect, leading to an increase in σ_b. When θ_u reached a threshold, the increasing θ_u began to dilute the salt concentration, resulting in a slight decrease in σ_b. More importantly, the variation of σ_b in the unfrozen zone can also help understand salt migration. For instance, as depicted in Fig. 7g, the change in the σ_b at the top sensor for the soil specimen with 2% salt content was negligible. It demonstrated that the salt flux was almost equal between the incoming and outcoming salt migrations under the coupling effect of convection and diffusion.

Pore water and salt redistribution were examined by sampling and tested after F-T. Fig. 8a illustrates the volumetric water content (θ) redistribution of soil specimens with different salt contents. The results were calculated by multiplying the gravimetric water content (ω) obtained by the oven-dry method with the specimen's dry density (ρ_d) and assuming a 100% degree of saturation. Moreover, the bottom and top sensors' locations and the final freezing front were also plotted in the figure to facilitate discussion. The ρ_d values after F-T were determined between 1.54 g/cm^3 and 1.64 g/cm^3, which were slightly less than the initial one (e.g., 1.65 g/cm^3) due to water inflow during F-T. The change in water content ($\Delta\theta$) was calculated as the absolute difference between the water contents before and after F-T. It can be seen that the θ values in both frozen and unfrozen zones increased for all but 4% salt content after F-T. The increase ranged from 0.005 m^3/m^3 to 0.02 m^3/m^3 at different heights, which agreed with and confirmed the reliability of the 5TE measured results. This observation can be explained by the fact that moisture migration still occurs within the frozen zone during freezing due to the much higher unfrozen water content than non-saline soil (e.g., 0.093 m^3/m^3 and 0.152 m^3/m^3 for the salt content of 1%, 2% compared with 0.017 m^3/m^3 for non-saline specimen at thermal equilibrium). The maximum increase occurred near the final freezing front, and the increases were more uniformly distributed among the entire specimen than reported for non-saline soils (Fan et al., 2019). The θ of 4% salt content decreased in the unfrozen zone and increased slightly in the frozen zone after F-T, as shown in Fig. 8a, which was consistent with the results presented in Fig. 7d, and the possible reason was also discussed previously.

The salt redistribution, as illustrated in Fig. 8b, was consistent with the measured σ_b in Fig. 7f-h and supplied data for other locations. Take

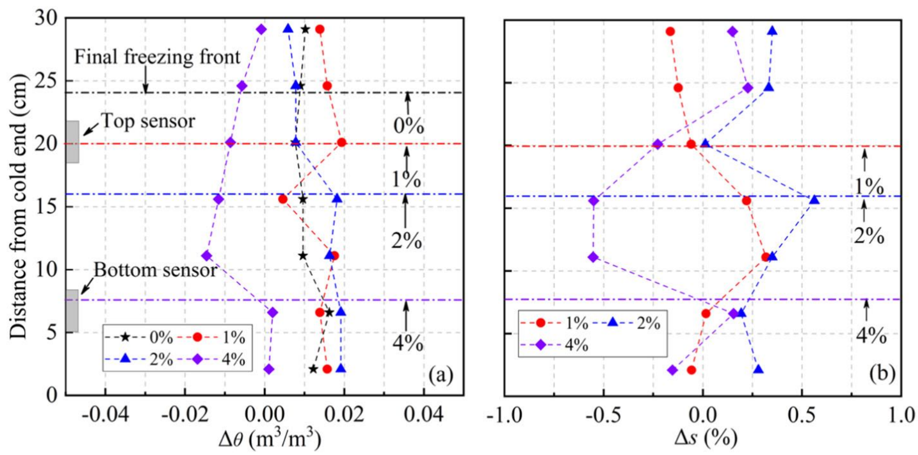

Fig. 8. Illustration of (a) water and (b) salt redistribution due to F-T for specimens with different salt contents. Note that the locations of the final freezing front, 5TE and matric suction sensors were shown for reference.

2% salt content as an example. The salt content at 6.6 cm from the cold plate increased slightly (refer to Fig. 8b), which agreed well with a slight increase in the σ_b after F-T at the bottom sensor shown in Fig. 7g. In contrast, the salt content at 20 cm from the cold plate did not change (Fig. 8b), which corresponded well with the almost constant σ_b throughout the entire F-T at the top sensor (Fig. 7g). Due to the coupling effect of convection and diffusion on salt migration, one can see a more complex salt redistribution pattern (Fig. 8a) than water content redistribution (Fig. 8b) after F-T. The salt content generally peaked near the finial freezing front except for the 1% salt content and dropped to reach the minimum at a certain distance above the freezing front, since the salt migration with water toward the freezing front due to convection dominated other factors. No such drop in the salt content occurred in the specimen with 1% salt content, likely due to an ample supply of NaCl solution to the zones above the freezing front close to the water supply. Additionally, salt was also able to migrate in the frozen zone toward the cold end via the relatively thick unfrozen water film in saline soils (Xiao et al., 2017; Hou et al., 2020). This observation is consistent with that from Baker and Osterkamp (1989), which observed an increase in the solvent in the frozen zone with a relatively high freezing rate (larger than 10 mm/day). The different patterns in the redistributed water content and salt content can be attributed to the complicated mechanism of salt migration, including convection and diffusion, compared with only one primary mechanism, i.e., convection, in water migration.

Understanding the relationship between θ_u and σ_b offers potential for in-situ monitoring of freezing and thawing. Fig. 9 depicts the relationship between θ_u and σ_b of specimens with 1% and 2% salt contents at the bottom sensor during F-T. Note that the measured σ_b or θ_u at other salt content or sensor locations only varied in a small range and was therefore not shown for clarity. The hysteresis phenomena can be observed in Fig. 9, indicating that the thermal path impact on the relationship between σ_b and θ_u. One can see in Fig. 9b that σ_b decreased even though the θ_u stay at 0.416 m^3/m^3, possibly due to reduced viscosity of pore water with a decreasing temperature during initial cooling. σ_b fell with a decreasing θ_u in the following freezing process. Specifically, θ_u decreased due to phase change from pore water to ice during freezing, resulting in fewer conducting pathways and hence a decrease in σ_b (Tang et al., 2020; Liu et al., 2020b). Once thawed, σ_b increased with an increasing θ_u and then changed far less. As the temperature rose during thawing, θ_u increased due to phase change from pore ice to water, forming more conducting channels and hence increasing σ_b. When most of the channels were connected, σ_b firstly reached a plateau and then varied due to more water-salt migration when θ_u kept increasing. The range of the unfrozen water content in which the σ_b remained constant was larger for the specimen of 1% salt content than 2%. At the end of thawing, both θ_u and σ_b increased compared with their initial values due to water and salt migration.

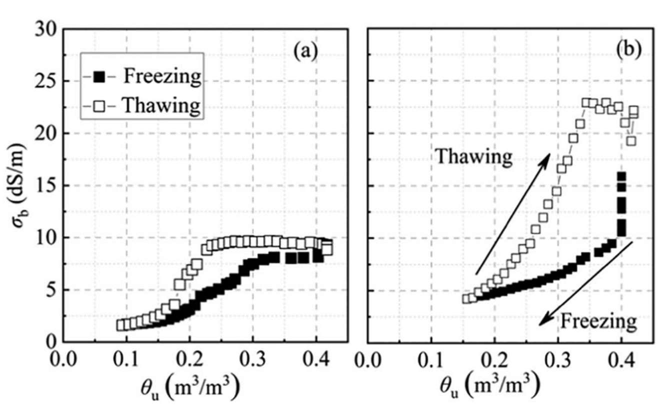

Fig. 9. Unfrozen water content vs. bulk electrical conductivity for specimens with different salt contents detected at the bottom sensor during F-T: (a) 1% salt content and (b) 2% salt content.

3.2.3. Matric suction

Investigation on the matric suction helps understand the driving force of water-salt migration. Fig. 10 shows the variation of ψ_m and temperature with time for specimens with different salt contents during F-T. Due to the large size of the matric suction sensor, the measured matric suction values represented the average within the area of 3.5 cm diameter that was directly in touch with the circular ceramic disc, as depicted in Fig. 3. From the data measured by the bottom matric suction sensor in the soil specimen with no salt shown in Fig. 10a, one can see that the ψ_m was minimal (around 13 kPa) before the freezing front arrived at the sensor; afterward, it increased substantially and reached to a peak value of 6006 kPa during freezing and dropped quickly to around 10 kPa during thawing. A similar trend can be observed from the results obtained at the top sensor. The maximum ψ_m measured by the top sensor was around 1500 kPa. The large difference in the matric suctions between different heights drove water and salt migration to the cold end. For all other soil specimens with different salt contents, as shown in Figs. 10b through d, the initial ψ_m values were around 10 kPa, indicating that ψ_m was relatively insensitive to salt content. This observation agrees with the finding of previous studies (e.g., Sun et al., 2013; Zhang et al., 2017c). However, the maximum values of ψ_m measured by the bottom or top sensors in the frozen zone decreased with increasing salt content due to the different θ_u values.

The results mentioned above indicated that ψ_m was dependent on θ_u, which is consistent with the finding of Lu et al. (2018). Fig. 11 illustrates

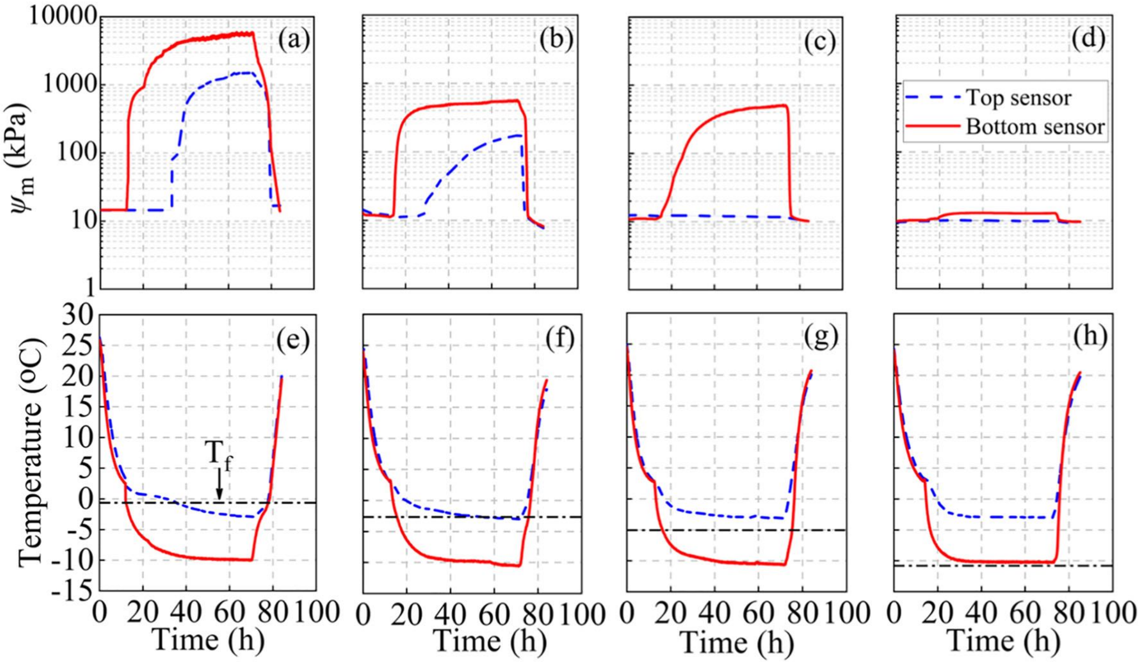

Fig. 10. Variation of the matric suction and temperature vs. time during F-T for specimens with various salt contents: (a) and (e): no salt; (b) and (f): 1% salt content; (c) and (g): 2% salt content; and (d) and (h): 4% salt content.

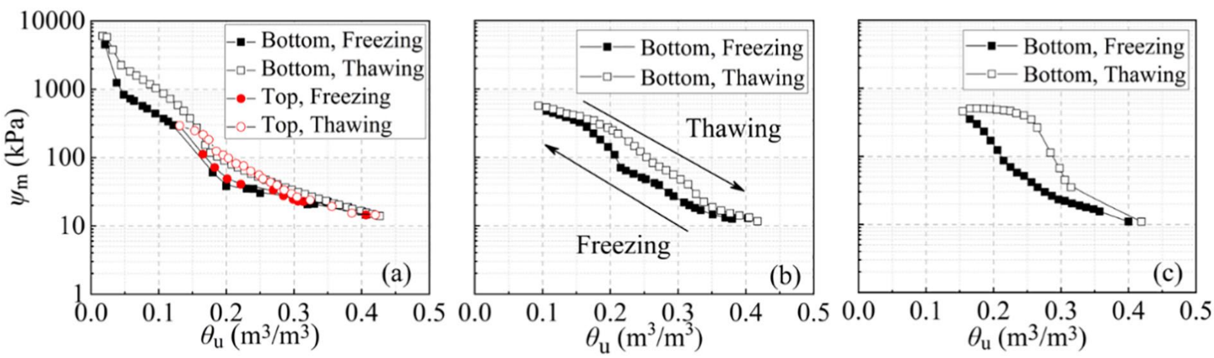

Fig. 11. The relationships between the unfrozen water content and matric suction for specimens with different salt contents during F-T: (a) no salt; (b) 1% salt content; and (c) 2% salt content.

the relationships between θ_u and ψ_m of specimens with different salt contents during F-T. Note that the results of the specimen with 4% salt content at both bottom and top sensors were not plotted due to the insignificant variation in θ_u. One can see that the ψ_m increased with a decreasing θ_u during freezing and then decreased with a rising θ_u during thawing (Fig. 11b). A significant hysteresis loop can be identified in a F-T cycle due to effects including the "ink-bottle" phenomenon, capillary condensation, non-steady-state nucleation, expansion and contraction, and electrolyte (Wang et al., 2018a). The loops were also not closed, similar to those in Fig. 9, due to the water and salt migration. Fig. 11a shows the θ_u-ψ_m loops of 0% salt content measured by the bottom and top sensors. At the thermal equilibrium state, the matric suction reached the maximum value of 6006 kPa (θ_u = 0.017 m^3/m^3) at the bottom sensor and 292 kPa (θ_u = 0.131 m^3/m^3) at the top one. The large matric suction gradient between these two sensor locations was the direct proof of the driving force of water and salt migration. Two loops were almost overlapped, indicating the uniqueness of the θ_u-ψ_m relationship for a particular soil. Therefore, only the θ_u-ψ_m relationships observed at the bottom sensor locations for specimens with 1% and 2% salt contents were plotted for clarity, and the hysteresis phenomenon was also evident (Figs. 11b and c). At the thermal equilibrium state, the ψ_m peaked at 6006 kPa, 564 kPa, and 458 kPa at the bottom sensor location for the specimens with 0%, 1%, and 2% salt content. This data showed that the matric suction gradient decreased with increasing salt contents, resulting in less water and salt migration. The matric suction data and the unique relationship between the matric suction and unfrozen water content in a certain soil revealed the magnitude of the driving force for water and salt migration. Future studies could focus on the quantitative relationship between matric suction and unfrozen water content under the influence of salt content and water supplement to understand the physical properties of frozen saline soils.

3.2.4. *Water intake*

It is crucial to monitor the water intake during F-T in an open system as this information can be useful for analyzing frost heave (Gilpin, 1980; Hermansson and Guthrie, 2005). Fig. 12 shows the total volume of water or NaCl solution of various salt contents. Note that there were some data gaps since the data was manually recorded, and no recordings were taken at night. However, these data gaps did not seem to affect the continuity of the intake data curves. The water began to supply once the freezing process started. One can see that the water intake volume data were almost zero over the first five hours for all specimens.

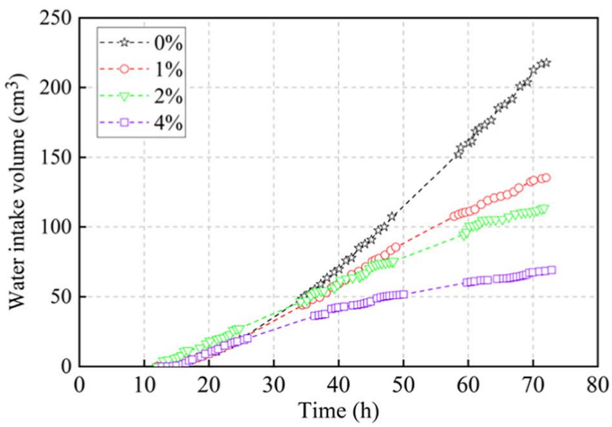

Fig. 12. Water intake volume vs. time for soil specimens with different salt contents during freezing.

Subsequently, the intake volume increased with time but was pretty close in the next ten hours for all specimens. Afterward, the water intake volumes started to rise almost linearly with time at different rates, and the differences between them grew over time. The larger volume occurred in specimens with lower salt contents. This observation is consistent with the results of Zhang et al. (2014). It indicated more water and salt migration in specimens with lower salt content due to the larger matric suction gradient. As previously discussed, a larger matric suction gradient in lower salt content between two sensors. Specifically, the maximum matric suction values at the thermal equilibrium state were 6006 kPa, 564 kPa, 458 kPa, and 13 kPa as measured by the bottom sensors and 292 kPa, 170 kPa, 13 kPa, and 13 kPa as measured by top sensors, for specimens with 0%, 1%, 2%, and 4% salt contents, respectively (Fig. 10). During thawing, the water and salt migrated under the effect of gravity and pore solution concentration gradient. The supplement water migrated to the freezing front and went through water-ice phase change in the frozen fringe, inducing frost heave. The water intake-induced frost heave was reported as the primary contributor to the total frost heave (Zhang et al., 2017a). A quantitative analysis of the deformation of frozen saline soils will be performed in a separate study due to page limits.

4. Conclusions

Unidirectional open-system F-T tests were conducted on saturated clay specimens with varying sodium chloride contents to investigate the water and salt migration mechanism. The test devices and sensor installation were described in detail. Testing results, including the relationship between temperature and time, development of the freezing front, the variation of unfrozen water content, bulk electrical conductivity and matric suction during F-T, and the water intake volume during freezing were presented. The relationships between the unfrozen water content and the bulk electrical conductivity or matric suction were also presented and analyzed to shed light on the water and salt migration. In addition, the NMR relaxometry tests were performed to examine the water molecule mobility for understanding the water-salt migration mechanism. The following conclusions can be drawn:

(1) The freezing front propagation was found to be highly dependent on salt content. The freezing front moved faster at the beginning of freezing and then gradually reached a plateau at the end of freezing. The final location of the freezing front at the thermal equilibrium stage was farther from the cold end of the specimen with lower salt content than that with higher salt content.
(2) A significant but asynchronous variation was found in the unfrozen water content and bulk electrical conductivity during F-T. This is because the mechanisms of salt migration included convection and diffusion. In contrast, only one primary mechanism, i.e., convection, drove water migration, as confirmed by the redistribution of water and salt. There is less influence of convection and diffusion on salt migration in the unfrozen zone farther away from the freezing front. However, convection is the dominant among the two mechanisms regardless of the distance from the freezing front.
(3) The water intake volume increased with decreasing salt content, which can be attributed to the driving force of water-salt migration, e.g., matric suction gradient. The matric suction was found to be dependent on the unfrozen water content but independent of salt content. Furthermore, a hysteresis loop was revealed in the relationships between the unfrozen water content and matric suction of frozen saline soils during F-T.
(4) The water molecule mobility was dependent on the unfrozen water content but independent of salt content. The pore water in specimens with different salt contents but the same unfrozen water content were found to have similar water molecule mobility. The hysteresis phenomenon was also identified in the variation of water molecule mobility with temperature during F-T. Nevertheless, the salt content has a significant effect on the soil freezing point depression, which further affects the matric suction and water molecule mobility.

This study delves into the water and salt migration mechanism during F-T, which is of great significance for understanding the coupled thermo-hydro-salt behavior of frozen saline soils. Besides, many factors, such as soil texture, dry density, salt type, and degree of saturation, affect the water-salt migration and warrant further investigation. Additionally, the quantitative relationship between the unfrozen water content and matric suction under the influence of salt content and water supplement should be investigated in future studies to understand the physical properties of frozen saline soils.

Declaration of Competing Interest

We declare that we have no financial and personal relationships with other people or organizations that can inappropriately influence our work; there is no professional or other personal interest of any nature or kind in any product, service and/or company that could be construed as influencing the position presented in, or the review of, the manuscript entitled.

Acknowledgment

This work was supported by the National Natural Science Foundation of China (Grant No 51478226 and 51878069) and the National First-class Disciplines Fund. The authors appreciate Jiangsu Product Quality Testing & Inspection Institute for the technical support on the salt content test and National Engineering Research Centre of Biomaterials for the support on NMR relaxometry test.

References

Baker, G.C., Osterkamp, T.E., 1989. Salt redistribution during freezing of saline sand columns at constant rates. Water Resour. Res. 25 (8), 1825–1831.
Banin, A., Anderson, D.M., 1974. Effects of salt concentration changes during freezing on the unfrozen water content of porous materials. Water Resour. Res. 10 (1), 124–128.
Bing, H., He, P., 2008. Experimental study of water and salt redistribution of clay soil in an opening system with constant temperature. Environ. Geol. 55, 717–721.
Bing, H., Ma, W., 2011. Laboratory investigation of the freezing point of saline soil. Cold Reg. Sci. Technol. 67 (1–2), 79–88.
Bing, H., He, P., Zhang, Y., 2015. Cyclic freeze-thaw as a mechanism for water and salt migration in soil. Environ. Earth Sci. 74, 675–681.
Bloembergen, N., Purcell, E.M., Pound, R.V., 1948. Relaxation effects in nuclear magnetic resonance absorption. Phys. Rev. 73 (7), 679–712.
Braun, B., Shuster, J., Burnham, E., 1979. Ground freezing for support of open excavations. Eng. Geol. 13, 429–453.

Cai, H.B., Liu, Z., Li, S., et al., 2019. Improved analytical prediction of ground frost heave during tunnel construction using artificial ground freezing technique. Tunn. Undergr. Space Technol. 92, 103050.
Campbell, G.S., 1988. Soil water potential measurement: an overview. Irrigat. Sci. 9, 265–273.
Chamberlain, E.J., 1981. Overconsolidation effects of ground freezing. Eng. Geol. 18 (1–4), 97–110.
Decagon Devices, 2010. 5TE Operator's Manual. Version 5. Decagon Devices, Inc, Pullman, WA. Available online at: http://www.decagon.com/assets/Manuals/5TE-Manual.pdf.
Drotz, S.H., Tilston, E.L., Sparrman, T., et al., 2009. Contributions of matric and osmotic potentials to the unfrozen water content of frozen soils. Geoderma 148 (3–4), 392–398.
Fan, W.H., Yang, P., 2019. Ground temperature characteristics during artificial freezing around a subway cross passage. Transp. Geotech. 20, 100250.
Fan, W.H., Yang, P., Yang, Z.H., 2019. Impact of freeze-thaw on the physical properties and compressibility of saturated clay. Cold Reg. Sci. Technol. 168, 102873.
GB/T 50123-2019, 2019. Standard for Soil Test Method. Ministry of Construction, Beijing, P.R. China.
Gilpin, R.R., 1980. A model for the prediction of ice lensing and frost heave in soils. Water Resour. Res. 16 (5), 918–930.
Hermansson, Å., Guthrie, W.S., 2005. Frost heave and water uptake rates in silty soil subject to variable water table height during freezing. Cold Reg. Sci. Technol. 43 (3), 128–139.
Hou, R.J., Li, T.X., Fu, Q., et al., 2020. Research on the distribution of soil water, heat, salt and their response mechanisms under freezing conditions. Soil Tillage Res. 196, 104486.
Huang, H., Liu, M.Z., Chen, C.F., et al., 2019. Laboratory studies on nitrate redistribution during the freezing process of a water-saturated sand system. Environ. Sci. Pollut. Res. Int. 26, 13818–13824.
Jessberger, H.L., 1980. Theory and application of ground freezing in civil engineering. Cold Reg. Sci. Technol. 3, 3–27.
John, S.J., 1981. State-of-the-art report — engineering practice in artificial ground freezing. Eng. Geol. 18 (1–4), 313–326.
Kelleners, T.J., 2020. Coupled water flow, heat transport, and solute transport in a seasonally frozen rangeland soil. Soil Sci. Soc. Am. J. 84 (2), 399–413.
Liu, J.P., Yang, P., Li, L., et al., 2020a. Characterizing the pore size distribution of a chloride silt soil during freeze-thaw processes via nuclear magnetic resonance relaxometry. Soil Sci. Soc. Am. J. 84 (5), 1577–1591.
Liu, J.P., Yang, P., Yang, Z.H., 2020b. Electrical properties of frozen saline clay and their relationship with unfrozen water content. Cold Reg. Sci. Technol. 178, 103127.
Loch, J.P.G., Miller, R.D., 1975. Tests of the concept of secondary frost heaving. Soil Sci. Soc. Am. Proc. 39, 1036–1041.
Lu, J.G., Zhang, M.Y., Zhang, X.Y., et al., 2018. Experimental study on the freezing-thawing deformation of a silty clay. Cold Reg. Sci. Technol. 151, 19–27.
Lundin, L.C., Johnsson, H., 1994. Ion dynamics of a freezing soil monitored in situ by time domain reflectometry. Water Resour. Res. 30 (12), 3471–3478.
Morgenstern, N.R., Nixon, J.F., 1971. One-dimensional consolidation of thawing soils. Can. Geotech. J. 8, 558–565.
Ohkubo, T., Ibaraki, M., Tachi, Y., et al., 2016. Pore distribution of water-saturated compacted clay using NMR relaxometry and freezing temperature depression; effects of density and salt concentration. Appl. Clay Sci. 123, 148–155.
Rui, D.H., Guo, C., Lu, M., et al., 2019a. Experimental study on water and salt migrations in clay under freezing effect. J. Glaciol. Geocryol. 41 (1), 109–115 (in Chinese).
Rui, D.H., Zhai, J.B., Li, G.Y., et al., 2019b. Field experimental study of the characteristics of heat and water transfer during frost heaving. Cold Reg. Sci. Technol. 168, 102892.
Sarsembayeva, A., Collins, P.E.F., 2017. Evaluation of frost heave and moisture/chemical migration mechanisms in highway subsoil using a laboratory simulation method. Cold Reg. Sci. Technol. 133, 26–35.
Stähli, M., Stadler, D., 1997. Measurement of water and solute dynamics in freezing soil columns with time domain reflectometry. J. Hydrol. 195, 352–369.
Sun, D.A., Zhang, J.Y., Song, G.S., 2013. Experimental study of soil-water characteristic curve of chlorine saline soil. Rock Soil Mech. 34 (4), 955–960 (in Chinese).
Taber, S., 1930. The mechanics of frost heaving. J. Geol. 38 (4), 303–317.
Tang, Y.Q., Xiao, S.Q., Zhou, J., 2019. Deformation prediction and deformation characteristics of multilayers of mucky cay under artificial freezing condition. KSCE J. Civ. Eng. 23 (3), 1064–1076.
Tang, R., Zhou, G.Q., Wang, J.Z., et al., 2020. A new method for estimating salt expansion in saturated saline soils during cooling based on electrical conductivity. Cold Reg. Sci. Technol. 170, 102943.
Tian, H.H., Wei, C.F., Tan, L., 2019a. Effect of freezing-thawing cycles on the microstructure of soils: a two-dimensional NMR relaxation analysis. Cold Reg. Sci. Technol. 158, 106–116.
Tian, H.H., Wei, C.F., Yan, R.T., 2019b. Thermal and saline effect on mineral-water interactions in compacted clays: a NMR-based study. Appl. Clay Sci. 170, 106–113.
Wagner, A.M., 2013. Creation of an artificial frozen barrier using hybrid thermosyphons. Cold Reg. Sci. Technol. 96, 108–116.
Wallis, S., 1999. Freezing under the sea rescues Oslofjord highway tunnel. Tunn. Undergr. Space Technol. 8, 19–26.
Walthert, L., Schleppi, P., 2018. Equations to compensate for the temperature effect on readings from dielectric Decagon MPS-2 and MPS-6 water potential sensors in soils. J. Plant Nutr. Soil Sci. 181, 749–759.
Wan, X.S., Yang, Z.H., 2020. Pore water freezing characteristic in saline soils based on pore size distribution. Cold Reg. Sci. Technol. 173, 103030.
Wan, X.S., Gong, F.M., Qu, M.F., et al., 2019. Experimental study of the salt transfer in a cold sodium sulfate soil. KSCE J. Civ. Eng. 23 (4), 1573–1585.
Wang, K., Wu, M.S., Zhang, R.D., 2016. Water and solute fluxes in soils undergoing freezing and thawing. Soil Sci. 181 (5), 193–201.
Wang, C., Lai, Y.M., Yu, F., et al., 2018a. Estimating the freezing-thawing hysteresis of chloride saline soils based on the phase transition theory. Appl. Therm. Eng. 135, 22–33.
Wang, Y.T., Wang, D.Y., Ma, W., et al., 2018b. Laboratory observation and analysis of frost heave progression in clay from the Qinghai-Tibet Plateau. Appl. Therm. Eng. 131, 381–389.
Wang, S.H., Wang, Q.Z., Xu, J., et al., 2019. Thaw consolidation behavior of frozen soft clay with calcium chloride. Geomech. Eng. 18 (2), 189–203.
Watanabe, K., Muto, Y., Mizoguchi, M., 2001. Water and solute distribution near an ice lens in a glass-powder medium saturated with sodium chloride solution under unidirectional freezing. Cryst. Growth Des. 1 (3), 207–211.
Wen, Z., Ma, W., Feng, W.J., et al., 2011. Experimental study on unfrozen water content and soil matric potential of Qinghai-Tibetan silty clay. Environ. Earth Sci. 66, 1467–1476.
Xiao, Z.A., Lai, Y.M., 2018. Study on water and salt transfer mechanism in saline soil under freezing-thawing and dry-wet conditions. Chin. J. Rock Mech. Eng. 37 (s1), 3738–3746 (in Chinese).
Xiao, Z.A., Lai, Y.M., You, Z.M., 2017. Water and salt migration and deformation mechanism of sodium chloride soil during unidirectional freezing process. Chin. J. Rock Mech. Eng. 39 (11), 1992–2001 (in Chinese).
Xu, X.Z., Wang, J.C., Zhang, L.X., et al., 1995. Mechanisms of Frost Heave and Soil Expansion of Soils. Science Press, Beijing.
Zhang, L.H., Ma, W., Yang, C.S., et al., 2014. Investigation of the pore water pressures of coarse-grained sandy soil during open-system step-freezing and thawing tests. Eng. Geol. 181, 233–248.
Zhang, M.Y., Zhang, X.Y., Xu, X.T., et al., 2017a. Water-heat migration and frost-heave behavior of a saturated silty clay with a water supply. Exp. Heat Transfer. 30 (6), 517–529.
Zhang, X.D., Wang, Q., Wang, G., et al., 2017b. A study on the coupled model of hydrothermal-salt for saturated freezing salinized soil. Math. Probl. Eng. 2017, 1–12.
Zhang, Y., Ye, W.M., Chen, Y.G., et al., 2017c. Impact of NaCl on drying shrinkage behavior of low-plasticity soil in earthen heritages. Can. Geotech. J. 54 (12), 1762–1774.
Zhang, X.Y., Zhang, M.Y., Pei, W.S., et al., 2018. Experimental study of the hydro-thermal characteristics and frost heave behavior of a saturated silt within a closed freezing system. Appl. Therm. Eng. 129, 1447–1454.
Zhang, X.D., Liu, S.W., Wang, Q., et al., 2019. Experimental investigation of water migration characteristics for saline soil. Pol. J. Environ. Stud. 28 (3), 1495–1505.
Zhou, J.Z., Wei, C.F., Li, D.Q., et al., 2014. A moving-pump model for water migration in unsaturated freezing soil. Cold Reg. Sci. Technol. 104-105, 14–22.